

Modelling the processes of cliff-top erosion and deposition under extreme storm waves

J.D. Hansom^{a,*}, N.D.P. Barltrop^b, A.M. Hall^c

^a Department of Geographical and Earth Sciences, University of Glasgow, Glasgow, G12 8QQ, UK

^b Department of Naval Architecture and Marine Engineering, Universities of Glasgow and Strathclyde, Glasgow, G4 0LZ, UK

^c Department of Geography, University of St Andrews, KY 16 9ST, UK

ARTICLE INFO

Article history:

Received 25 October 2007

Received in revised form 18 February 2008

Accepted 20 February 2008

Keywords:

cliff-top quarrying and erosion
modelling extreme storm wave impacts
wave-tank experiments
cliff-top boulder deposition
palaeo-tsunami

ABSTRACT

At exposed sites on the deep water coasts of the British Isles, cliff-top storm deposits (CTSDs) occur on cliffs at a variety of elevations above sea level and may occasionally reach up to 50 m above sea level. Time-series field mapping of CTSDs has demonstrated their formation over the historical period and their continued modification during major past storms. This paper seeks to clarify the morphogenetic context of CTSDs, model the wave conditions and forces encountered at the cliff-face and cliff-top platform and propose mechanisms to link wave processes to cliff-face quarrying and landwards cliff-top transport of quarried blocks to deposition zones at the rear of the cliff-top platform. We report on wave-tank experiments using scaled cliff and wave conditions from a cliff in the Shetland Islands to focus on three situations: incident waves lower than the cliff edge height; at the same height as the cliff edge height; and higher than the cliff edge height. The modelling suggests that steep waves of 10 m and above impacting on a 15 m high cliff will result in impact pressures sufficient to promote crack propagation, block detachment and lifting of large blocks. Large, but not necessarily steep, waves of the same height as the cliff edge produce sufficient impact pressures and water flow over the cliff edge and platform to entrain blocks, transport and deposit them on the cliff-top. Where cliff-top height is below wave crest elevation “green water” bore flow occurs, sufficient to force rotation or lifting of blocks out of cliff-top and cliff-top platform ‘sockets’. High flow velocities rapidly accelerate and transport blocks inland until the flow attenuation results in deposition of blocks at the limit of run-up. The model results provide a good explanatory framework to account for the quarrying of the upper part of the cliff-face and cliff-top platform under storm wave conditions and provide an insight into the exceptional velocities experienced over the cliff-top platform under bore flow conditions. The modelling results show that extreme storm waves are capable of quarrying, transporting and depositing large blocks at altitude and significant distances inland and so present serious questions about the use of such deposits as diagnostic of palaeo-tsunami.

© 2008 Elsevier B.V. All rights reserved.

1. Introduction

Severe wave conditions occur during storms in the North Atlantic and it is not uncommon for deep water waves in the sea areas to the west of the Shetland Islands to achieve maximum heights of 20 m or more (BPX, 1995). Normally, substantial attenuation occurs as these waves shoal and refract into shallower coastal waters and this results in lower incident wave heights than would occur at sea (Trenhaile, 1997). However, in widely distributed locations along the western and northern seaboard of the British Isles, there exists extensive geomorphological evidence to suggest that the assumed significant attenuation of deep water waves in the nearshore zone is not universal (Hansom, 2001; May and Hansom, 2003; Williams and Hall, 2004; Hall et al., 2006). This evidence relates to the occurrence of water-washed and scoured surfaces often covered with substantial

accumulations of large boulders that have been deposited either individually or as small imbricate clusters at up to 35 m O.D., together with more organized landforms such as boulder ridges at up to 20 m O.D., collectively termed cliff-top storm deposits (CTSDs) (Fig. 1). The characteristics and distribution of CTSDs reported by Hall et al. (2006) allow the basic conditions that allow the development of these boulder accumulations to be identified as follows:

1. CTSDs require full exposure to storm waves coupled with deep water offshore;
2. the waves are capable of overtopping 10–30 m high cliffs and generate cliff-top forces sufficient to fracture bedrock and to detach and lift boulders as large as 277 m³; and
3. cliff-top rock platforms and ramps are washed by fast-moving bores capable of transporting boulders of up to 40 m³ over tens of metres inland.

Based on extensive field evidence detailed in three linked papers (Hall et al., 2006; Hall et al., 2008; Hansom and Hall, in press), we seek

* Corresponding author.

E-mail address: jim.hansom@ges.gla.ac.uk (J.D. Hansom).

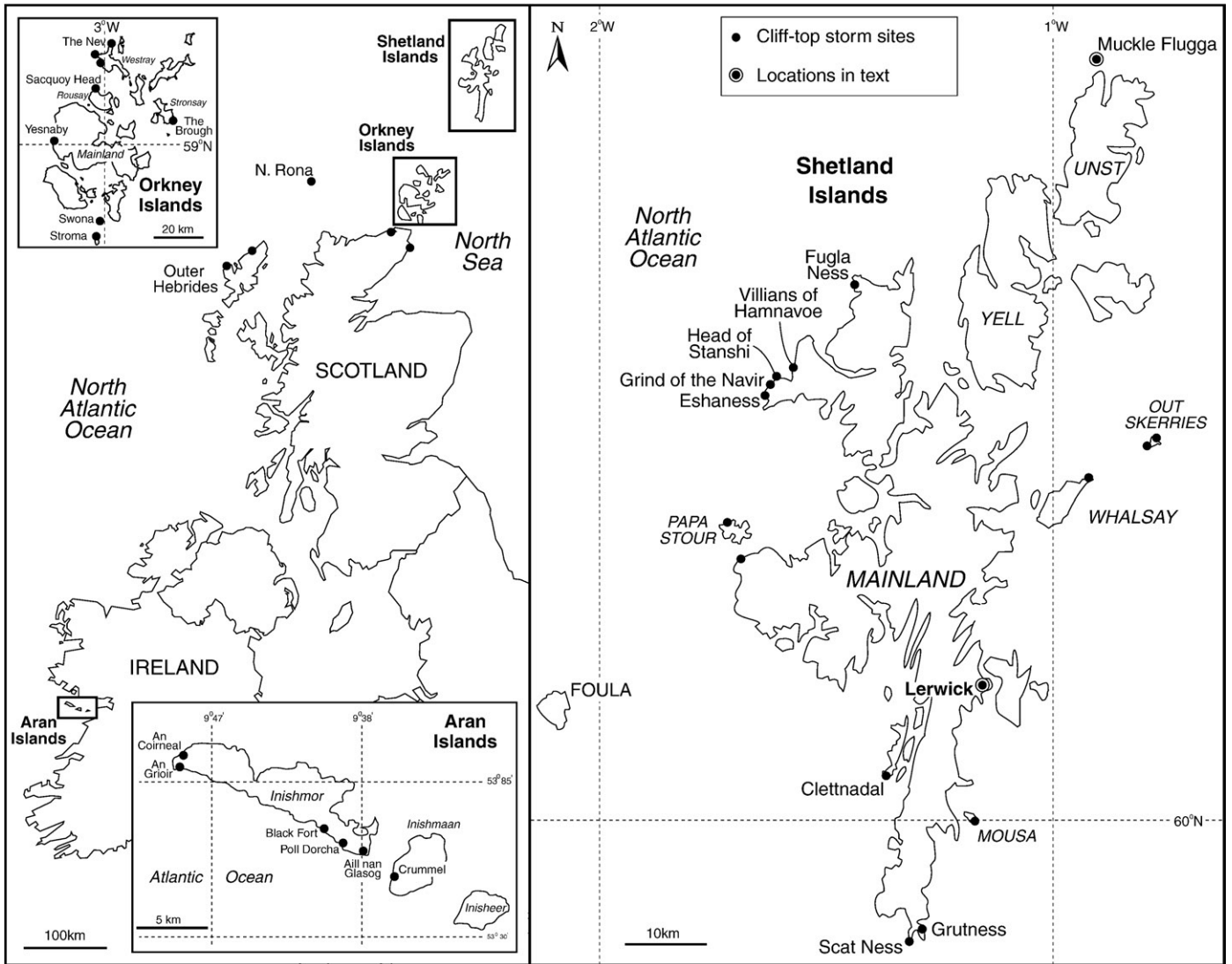


Fig. 1. Location map of known CTSDs on the coast of the British Isles including the sites covered here (from Hall et al., 2006).

here to model the waves that produce CTSDs. We focus on a sample site characterised by wave quarrying and organized cliff-top boulder ridges at The Grind of the Navir (The Grind), near Eshaness, in the Shetland Islands. Since the nearshore bathymetry, onshore topography, geomorphological processes and development chronology of this site have been previously established by Hall et al. (2008) and Hansom and Hall (in press), it was selected as a suitable site for physical wave-tank modelling using both scaled waves and cliff geometry in order to:

1. clarify the morphogenetic and wave climate context of CTSDs;
2. model the wave conditions and forces encountered at the cliff-face and cliff-top platform; and
3. propose mechanisms to functionally link wave processes to the quarrying of blocks from the cliff-face and top, transport these blocks landwards over the cliff-top platform, and deposit them at the rear of the cliff-top platform.

2. Constraining model parameters

The parameters for wave-tank modelling were derived from data on wave environments offshore of Shetland, from the geomorphology of CTSD sites in the British Isles and from evidence of the processes and forces involved in cliff-top erosion and transport at The Grind site in Shetland.

2.1. Wave environment

2.1.1. Winds

A characteristic feature of the Shetland climate is the frequency of strong winds. The mean annual wind speed is 6.5–7.5 m s⁻¹ and gales occur on average for 58 days per year mainly from the southwest, but the northwest and north are significant secondary directions (Barne et al., 1997). Between 1933 and 1993, December and January were the stormiest months and six storms were recorded at Lerwick in which gusts exceeded 44.6 m s⁻¹ (161 km h⁻¹), two of these being the most severe storms of the 20th century. During the storm of 1/1/1992, the highest hourly mean wind speed was 25.5 m s⁻¹ (92 km h⁻¹) from the west at Lerwick, with the highest gust reaching 34.7 m s⁻¹ (125 km h⁻¹) (data from the Meteorological Office). The same storm produced an unofficial UK record when a 67 m s⁻¹ (242 km h⁻¹) gust was recorded at Muckle Flugga, Unst (67 km northeast of The Grind).

2.1.2. Offshore wave environment

The wave environment in this part of the northeast Atlantic is extreme. During storms in 1969, the significant wave height (Hs) (the average of the highest third of all waves over 20 min) reached 18.5 m at 56°N, 4°W to the east of Shetland (Burridge, 1973) and in 1974 reached 15.13 m at 60°N, 4°W to the west of Shetland (Marex, 1975).

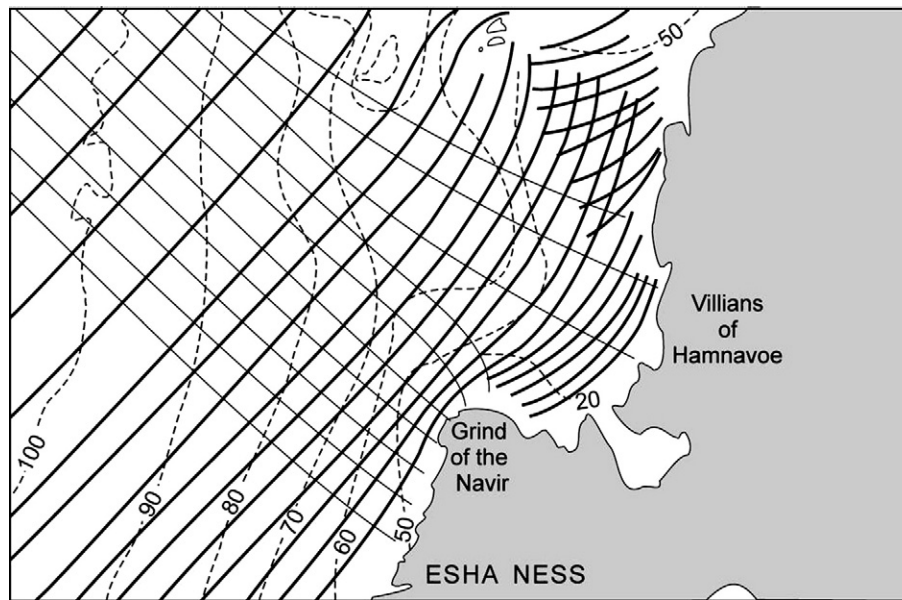


Fig. 2. Nearshore bathymetry and refraction model of the approach of waves of direction 314° , height 20 m ($1.51 H_s$), period 15 s T_z at The Grind field site, Eshaness, Shetland. Depths in metres.

The most probable highest individual wave (H_{mpm}) in a 3-hour storm is about $1.86 H_s$ and on 1.1.1995, at Statoil's Draupner gas platform in the North Sea, the so-called "January Wave" H_{mpm} was measured by laser to be 26 m. Also in 1995, the BP Amoco platform Schiehallion, 160 km west of Eshaness, Shetland, was struck by a wave that ruptured the fo'c'sle 18 m above the waterline (Lawton, 2001). Modelling of extreme waves in deep water at Schiehallion suggests that wave heights of 20 m occur about 100 times per year (BPX, 1995), the same data producing a 1-year maximum individual wave height (H_{max}) of 24.3 m (BPX, 1995). Nearby, wave buoy data (K7 at $60^\circ 42' N$, $4^\circ 30' W$, www.ndbc.noaa.gov/station_page.php?station=64046) supports this with the highest individual waves during storms on 1/1/1992 and 17/1/1993 reaching 28 m and 21 m respectively. Such waves are the same order of magnitude as those recorded in 2004 in the Gulf of Mexico under Hurricane Ivan, where an individual H_{max} reached 27.7 m (Wang et al., 2005) and in February 2000 near Rockall 250 km west of Scotland, where an individual H_{max} reached 29.1 m (the highest individual wave ever recorded) (Holliday et al., 2006).

There is also evidence to suggest an increase in wave heights in the North Atlantic over recent decades. The Waves and Storms in the North Atlantic (WASA) project used a combination of modelling and observational data to report increases in wave height of $2.5\text{--}7.5 \text{ mma}^{-1}$ over the period 1955–94 (Gunther et al., 1988). This is supported by observational data indicating a $1\text{--}3 \text{ mma}^{-1}$ increase in North Atlantic wave height over the last 30 yr, possibly linked to NAO intensification (Gulev and Hasse, 1999). If this is the case then it is likely that the maximum height of extreme waves has been subject to increase over recent years.

2.1.3. Nearshore wave environment

Shorelines with CTSDs generally have deep water offshore but lack nearshore skerries or wide shore platforms. In order for extreme offshore waves to be capable of modification of Shetland cliff-tops, only limited nearshore wave attenuation can occur. This is possible at The Grind since much of the seabed offshore lies at about ~ 100 m although within 2000 m offshore of the cliffs the gradient steepens to reach water depths of ~ 50 m at 500 m and ~ 20 m at 200 m (Fig. 2).

The mean orientation of the long axes of imbricate cliff-top boulders on the Shetland cliff-tops (Table 1) can be used as an estimate of the approach direction of the storm waves responsible for

replacing the boulders and at The Grind site this direction is 314° (approximately west-northwest). Refraction modelling of a 20 m high and 15 s period wave (derived from the BPX (1995) Schiehallion data) from 314° produces only limited rotation of the wave fronts of 5° to bring them sub-parallel to bathymetric contours (Fig. 2). Orthogonal convergence at The Grind (refraction coefficient of 1.2) results in a 20% increase in wave energy levels. Bartrop and Adams (1991) suggest that a 20 m and 15 s wave is likely to commence breaking in 20–30 m of water and at The Grind with a shoaling coefficient close to 1, a breaker of about 20 m high will begin to spill in about 28 m of water (Bartrop and Adams (1991)).

On the open coast in the Shetland Islands spring tidal range is limited to 1.5 m and maximum tidal currents on spring tides are generally between 0.5 and 1.25 m s^{-1} although higher values are achieved within inlets and bays (Barne et al., 1997). The effect of tidal flows on the open coast is mainly restricted to modification of wave heights particularly when in opposition to wave approach direction. In the context of the study site CTSDs, tidal effects are regarded to be of negligible importance, since the directions of flood and ebb are generally coast-parallel and the offshore wave approach directions are generally approximately coast-normal.

Table 1

Coastline orientation and preferred orientation of wave-deposited imbricate blocks on northwest Shetland cliff-tops

Location	Altitude (m)	Coastal orientation ($^\circ$)	Mean orientation of boulder long axis ($^\circ$)	Number of boulders	Mean long axis (m)
Virida Field, Papa Stour	35	5	300	15	0.7
South Head	25	360/0	315	25	1.1
Villians of Hamnavoe	17–22	10	302	47	0.8
Grind of the Navir 1	19	360/0	314	20	1.2
Grind of the Navir 2	20	360/0	290	25	0.7
Esha Ness	35	20	275	15	1.0

Based on this, subsequent wave modelling used a dominant approach direction of 314° (from May and Hansom, 2003).



Fig. 3. Grind of the Navir, Esha Ness, Mainland, Shetland where 15–22 m high cliffs are regularly overtopped during storms, leading to quarrying of the cliff-face and cliff-top platform and transport of large blocks landward.

2.2. Cliff profile

CTSD sites show a sequence of morphogenetic zones of varying width, comprising cliff, cliff-top wave scour zone, boulder accumulation zone and a landward zone characterised by wave-splash and air-throw debris (Hall et al., 2006).

2.2.1. Cliff-face

The most common profile is of a flat or gently ramped cliff-top fronted by a near-vertical cliff > 10 m high that extends to depth well below low water mark (Fig. 3). In planform the cliff-face is often penetrated by narrow clefts, known as geos, along lines of geological weakness. At The Grind, geos act to focus wave energy on parts of the cliff-top (Hall et al., 2008).

2.2.2. Cliff-top wave scour zone

The cliff-top rock platforms and ramps are largely swept clear of debris by storm wave activity. In the Eshaness area of Shetland, 40–150 m wide wave-scoured rock platforms occur at Villians of Hamnavoe (Mactaggart, 1999). At the headland of The Grind, the 15–20 m high cliffs are regularly overtopped in major storms and the 40–60 m wide cliff-top platform quarried by waves (Hall et al., 2008).

2.2.3. Boulder accumulation zone

Boulders quarried from the cliff-top platform are transported landwards and deposited at the rear, with carry distances of 10–50 m along paths that are clearly traced by striations produced as the in-transit boulders impact on the platform surface. The boulder accumulation zone may comprise individual clasts, spreads and ridges that extend inland of the limits of modern storm wave wash onto vegetated cliff-top surfaces. Locally, the CTSDs may be boulder ridges that are generally arcuate in planform mirroring the planimetry of the fronting cliff edge, with boulder imbrication generally conforming to the approach direction of waves over the cliff-top. For example, at The Grind, a fine sequence of eight boulder ridges occurs at 15 m O.D., the largest of which is up to 3.5 m high and composed of ignimbrite boulders up to 2.5 m *a*-axis (Fig. 4).

2.3. Cliff-top erosion and transport at The Grind

2.3.1. Bedrock fracturing

The ignimbrites at The Grind dip 5–10° inland and the coastal orientation follows approximately the strike of the rocks. Thus an

approximately rectilinear geometry is presented to waves approaching from the west and northwest. In addition, the ignimbrites at The Grind are jointed in both the horizontal (mean spacing 0.7 m) and vertical dimension (mean spacing 0.6 m) and are thus likely to be susceptible to weakening and detachment under severe wave conditions (Hall et al., 2006) (Fig. 5). Fresh fractures that cut across joint sets have been observed on the cliff-face and on rock steps on the cliff-top platform after major storms at The Grind. These fractures indicate that waves breaking on the cliff-face and cliff-top generate forces sufficient to fracture bedrock. The tensile strength of the host rock is about 10% of its compressive strength (approximately 1.5 MPa for ignimbrite) (Sunamura, 1992) and if exceeded, wave impact pressure acting in conjunction with air compression into joints, is a very effective erosional process (Trenhaile and Kanyaya, 2007), even under much lower waves than experienced at The Grind.

2.3.2. Block quarrying

The cliff-face at The Grind shows stepped overhangs with fresh and weathered scars indicating progressive upwards removal of rock slabs from the cliff-face. It is inferred that during storms up-rushing wave water is capable of entering joints between and behind the slabs and forcing them from the cliff-face (Sunamura, 1992).



Fig. 4. A prominent 3.5 m high CTSD ridge at Grind of the Navir, 50 m inland of the cliff edge at 17 m above sea level. Rucksack for scale.



Fig. 5. Detail of the fracturing of cliff-top bedrock surfaces at 16–18 m above sea level at Grind of the Navir following the January 2005 storm. Overtopping water from subsequent storm waves then removes the blocks and transports them landward.

Cliff-top scoured zones often show fresh scars and sockets where recent block removal has occurred after quarrying by storm waves (Fig. 5). Sharp-edged scars and sockets are most common at the cliff edge and on the seaward side of small rock steps on the cliff-top platform: the preferred sites for quarrying of blocks by waves. For example, in storms in the early 1990s, quarry zones at Villians of Hamnavoe released blocks of up to 1.8 m³. During the same storms at The Grind, boulders of ignimbrite up to 0.64 m³ were removed leaving multiple sockets with fresh joint-bounded surfaces. The largest socket known is from the Aran Islands, Ireland and measures 18 × 11.5 × 1.4 m (Williams and Hall, 2004).

2.3.3. Block transport

Matching transported blocks to sockets indicates that blocks are lifted, flipped and rotated out of sockets. The small numbers of blocks retained in the cliff-top scour zone indicate that wave energy on the cliff-top is also sufficient to carry blocks 10–60 m inland to the boulder accumulation zone, which is sometimes marked by a boulder ridge or series of ridges (Fig. 4). Patterns of sockets and scars on The Grind indicate that water depths on the cliff-top when extreme waves impact are < 10 m deep and were < 4 m deep in a storm in 2005. The boulder accumulation zones at the rear of the cliff-top scour zones may be at similar or even higher elevations than the apex of the cliff-top, indicating shallow water depths. These observations are consistent with the generation of fast-moving bores of wave water on the cliff-top during storms.

The maximum size of boulders in the boulder accumulation zone constrains the entrainment forces operating within these bores. Blocks of up to 1.2 m³ occur at The Grind and are comparable with block sizes common at other CTSD sites. These block sizes are small, however, when compared with largest CTSD blocks known. Blocks of tuff up to 277 m³ occur at Villians of Hamnavoe, Shetland, and blocks of limestone up to 96 m³ occur on the Aran Islands, Ireland. This disparity reflects the tendency of fractured rocks to fragment during wave transport.

3. Modelling wave impacts and dynamics on the cliff-face and cliff-top

In this project, these data were used to generate Froude scaled deep water waves which were then allowed to impact onto simplified scaled physical cliff models in wave tanks.

3.1. Impact pressures and cracking of the cliff-face to form blocks

We have not attempted to measure the pressures within cracks that might cause fracturing. However, large pressures are known to act

in cracks subject to wave impact loads (Müller et al., 2003) and on breakwaters landward forces generated by breaking waves within 10 mm wide cracks can reach 55 MPa (5500 m of head) (Peregrine et al., 2004). Measurements during wave impacts on Alderney Breakwater, Jersey, record the development of seaward pressures at the end of cracks of up to 25 MPa (2500 m of head) (Peregrine et al., 2004). Field results during storms on sloping shore platforms at sea level show that under breaker heights as low as 2 m, impact pressures at the mouths and inside of cracks match those of Müller et al. (2003) and are sufficient to dislodge and move blocks (Trenhaile and Kanyaya, 2007).

Trenhaile (1987) considers none of the many models that estimate the wave pressures exerted on a cliff by breaking and broken waves to be fully satisfactory. Deriving a single expression relating wave impact to wave or breaker height has been problematic, probably on account of instabilities in the breaking wave and the range of boundary conditions used, as well as differences in experimental technique and equipment (Trenhaile, 1987). More recently, Sunamura (1992) has considered the impact of a vertical wave front on a cliff-face and produced results that are consistent with similar earlier work by others (e.g. Denny, 1951). Sunamura (1992) shows that a vertical wave front produces maximum pressure on a cliff, this being composed of both dynamic and hydrostatic components. The static pressure at the position of maximum dynamic pressure is negligible but the maximum dynamic pressures exerted on a cliff submerged by breaking waves can be estimated from Sunamura (1992):

$$p_m = 35\rho_f g H_{ob}$$

where

ρ_f	mass of unit volume of water (1024 kg m ⁻³)
H_{ob}	deep water wave height
g	9.81 m s ⁻²
p_m	max dynamic pressure.

For The Grind, $H_{ob} = 20$ m, shoaling coefficient = 1, so $p_m = 7$ MPa (or 700 m head of water).

Similar ratios of maximum pressure to wave height were found by Denny (1951), these values occurring where the vertical front of a breaking wave hits a cliff, the maximum pressure typically occurring at an elevation of about 30% of the wave height below the crest, an observation echoed by several workers (Trenhaile, 1987). Pressures are roughly halved by ripples on the water surface (Denny, 1951) and rough rock surfaces would also reduce these pressures so a maximum pressure of 3.5 MPa (350 m head) might be a more realistic estimate.

Lower average pressures from breaking waves are given by Homma and Horikawa (1965a,b):

$$p_b = 2.8\rho_f g h_w$$

where h_w is the water depth at the cliff.

For The Grind, $h_w = 10$ m, so $p_b = 0.28$ MPa (or 28 m head).

It is interesting that these very different pressures with 20 m high waves are similar to the wide range of observed local peak pressures (450 m head over an area about 0.05 m², 200 m head over 1.8 m² and 25 m head over several hundred m²) measured in oil production barge bow-breaking wave impact tests (Xu and Barltrop, 2005). Although, the barge results were obtained with 30 m high deep water waves, this may be offset by the tendency of deep water waves to break less violently than shoaling waves. Some of the differences in observed pressures may also be a result of the different frequency responses of the measuring equipment.

Noormets et al. (2004) suggest that if the pre-impact fracture occupies more than 60% of the failure plane (i.e. less than 40% is attached) then the propagation of cracks in the rock face and the potential for subsequent rock failure is enhanced. This is due to wave

impact pressure and internal pressure acting via air compression in the joints, cracks and other discontinuities and appears to be a common condition at The Grind. The waves causing fracture propagation can themselves detach and transport the block or may leave it susceptible to transport by a later and possibly lesser wave that could not itself have fractured the rock face. Closed fractures in the rock of the cliff-face are widened by the removal of rock chips, allowing small prismatic blocks to be removed from otherwise planar rock surfaces, a process analogous to the loss of masonry blocks seaward from sea walls and breakwaters (Marth et al., 2005). At The Grind, using conservative wave-derived cliff-face pressures of 3.5 MPa (350 m head), the tensile strength of the rock (1.5 MPa) is greatly exceeded, the impact pressure sufficient to create fracturing and the internal pressures within cracks further propagating any cracks in the rock. Since the rock face at The Grind is already joint and crack-defined then the high internal pressures achieved are capable of detaching adjacent blocks where no cohesion exists, and especially at the apexes of the cliff or platform where no constraining overburden exists.

The very high pressures are typically of short duration (0.001 to 0.01 s) and affect a very small area of the rock face at any one time. Our calculations show that whilst this high pressure may dislodge a block and move it into a flow that will transport it, the pressure duration is too short to have a significant effect once the block is actually in transport.

3.2. Model tests

Model tests were performed to gain some understanding of the nature of wave breaking at the cliff and to establish the conditions required to transport blocks inland from the cliff edge. Three short series of model tests were performed:

1. Waves impacting the cliff below the cliff edge;
2. Waves crests impacting approximately at the cliff edge; and
3. Waves overtopping the cliff edge.

The tests were performed using Glasgow and Strathclyde Universities' wave-tank facilities. The first two tests were in a 74 m×4.6 m×2.2 m

water depth wave tank. The third set of tests was performed in a smaller 25 m×1.5 m×0.6 m water depth tank. In the large tank a sloping sea bed was used, however the bathymetry immediately in front of The Grind cliff is uncertain and so constructing a highly accurate model was not practicable. Once the bathymetry is fully established, additional tests are planned to determine the sensitivity of the wave behaviour.

The tests are summarised in Table 2 with the dimensions and results given at prototype scale using Froude scaling. (Some model scale dimensions are also given in the text in square brackets.) Froude scaling maintains the correct ratio of inertia to gravity forces and is necessary for this type of experiment. Viscous forces, capillary forces and air compressibility will not be properly scaled. Viscous effect (Reynolds number scaling) errors local to the cliff are of low significance since the blocks are square-edged rather than rounded, resulting in lower sensitivity to an incorrect Reynolds number. Capillary forces (Weber number effects) will be negligible for waves at both full and model scale but in the vicinity of a breaking crest it is likely that the capillary forces will hold the wave together, making the profile more rounded and reducing spray. Air compressibility (Cauchy number) is important when steep wave impacts trap air between the cliff-face and the wave. However this is probably less important for block movement than for the prediction of peak pressures that might cause fracturing of the rock. Froude scaling between the model and the full scale, results in pressures that are proportional to length, forces proportional to length cubed and time inversely proportional to square root of length.

The first tests were at a scale of 1:30 with the aim of establishing some understanding of how waves, especially large breaking waves, interacted with the cliff. A 1:20 slope steepened to 1:5, 96 m [3.2 m] in front of the cliff. The slope extended the full 138 m [4.6 m] width of the tank. The cliff model itself was 72 m [2.4 m] wide but vertical walls extending 45 m [1.5 m] in front of each side of the cliff model water encouraged two-dimensional flow in the vicinity of the cliff. The water depth in front of the cliff in the model was 18.75 m [0.625 m]. The water depth immediately in front of The Grind cliff is uncertain but deeper water will allow higher waves to reach the cliff without

Table 2
Summary of wave-tank model tests and results

	Model test 1	Model test 2	Model test 3
Scale	1:30	1:60	1:375
Cliff height	15 m	15 m	15 m
Cliff front	Vertical	Vertical	Vertical
Cliff-top	Horizontal	Horizontal	Horizontal
Water depth at cliff	18.75 m	12 m	15 m
Water depth at wave paddle	66 m	132 m	225 m
Seabed slope	1:5 at <64 m from cliff 1:20 at >64 m from cliff	1:20	1:6
Instruments	Video	Video	Video
	Wave probes	Wave probes Force transducer (4320×960×960)	
Block dimensions (m)	1.6×0.8×0.24	3.2×1.6×0.5 2.1×1.2×0.4 1.5×0.9×0.3	No rock blocks
Wave types	Wave groups Breaking below cliff edge	Wave groups Breaking at cliff edge	Regular waves Wave flow over cliff-top
Observed cliff-top flow	The initial flow is a near vertical jet which then angles landward to land on cliff-top. Results in a return flow seaward over the cliff edge. Landward flow occurs but with longer flow paths and less intense flow.		Strong landward flow (drainage possible behind the cliff).
Findings	Incoming wave breaks on reflected wave and reflection increases wave height at cliff. Blocks dislodge if not set back from the cliff face. Most blocks carried upward and landward. Some may move seaward.	Wave forces on transducer easily capable of moving large blocks. Most blocks carried upward and landward. Very few move seaward.	Initial bore of water moves rapidly over the cliff edge landward: bore flow similar to dam break flow. Bore flow is followed by a solitary wave. All blocks lifted and transported substantial distances landward.
Resultant hypotheses	Greatest impact force on upper cliff when large wave follows small wave.	High breaking waves favour landward block movement.	Overtopping by high waves produces bore flow that transports all blocks landward.

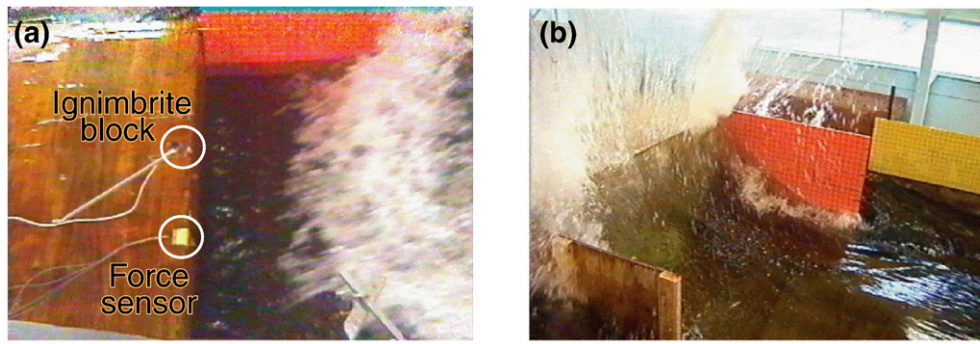


Fig. 6. a: Video-still of model cliff-top with approaching breaking wave. Scaled block and pressure transducer indicated. b: Model cliff-top shortly after breaking wave impact. 1:30 scale tests.

breaking and so for these first tests the water was deeper than it was likely to be in practice, preventing breaking induced by shallow water. The cliff height above the mean water level was scaled to represent 15 m above the water level. A machined cuboid of Grind of the Navir ignimbrite was inserted into a recess in the leading edge of the cliff-top corner. The water surface elevation was measured in front of the cliff and in deep water using two 2-wire resistance gauges, measurement of the water surface shape was via a square grid on the tank side and the tests video-recorded (Fig. 6a and b).

The second tests were at a scale of 1:60 on a constant 1:20 slope. The slope extended across half the width of the tank 138 m [2.3 m] and a central longitudinal wall 1560 m [26 m] long and the tank side prevented water flowing off the slope. The cliff extended the full width of the slope. The water depth at the cliff toe was 12 m and the cliff height 15 m. Three machined Grind of the Navir ignimbrite blocks (see Table 2) were inserted into recesses in the cliff-top corner. A force sensor was installed in the cliff edge. At this scale it represents 4.32 m (along the cliff edge) × 0.96 m (to landward) × 0.96 m (vertically). Again water surface elevation was measured at the cliff and in deep water and the tests videoed.

A third set of tests were undertaken in a small tank. This set of tests was performed at a scale of 1:375 on a slope of 1:6. The objective was to visualise the overtopping of the cliff by waves with an incident elevation about equal to the cliff height. Water depths of 15 m and cliff height of 15 m were used and the results videoed.

3.3. Wave conditions and water surface elevations observed in the model tests

The first model tests demonstrated the importance of wave reflection for wave crests orientated parallel to the cliff edge.

Similar to real sea conditions, the tests used irregular waves, generated in deep water using a JONSWAP (Hasselmann et al., 1973) spectrum. We were interested in wave impact and anticipated that waves breaking on the cliffs were required so generated deep water sea states including relatively steep ($H_s/gT^2 = 1/13$) seas and allowed these waves to propagate to the cliff. To reduce testing time extreme wave groups representing average extreme 1 in 3-hour conditions at the cliff, rather than a long series of waves, were generated. The wave groups containing the highest waves were based on New Wave Theory (Tromans et al., 1991) and other wave groups including steepest waves used a modified New Wave Theory (Xu and Barltrop, 2005).

In low steepness regular waves, reflection causes the well-known sinusoidal standing wave condition (clapotis), which approximately doubles the local wave height at the cliff and results in wave particle motions that are parallel to the cliff-face.

In tests with steeper waves, a large increase in local wave height occurred but progressive waves towards the cliff appeared to be more dominant than standing waves. Often the incoming wave would break on meeting the previous reflected wave, progress towards the cliff as a

bore and then surge up the cliff-face. Even if the wave did not break before the cliff-face the resulting water surface shape surging up the front of the cliff was concave in contrast to the convex surface predicted for a linear clapotis.

The size of the wave preceding the potentially damaging wave is important because its reflection from the cliff interacts with and may break the wave before it reaches the cliff. The size of the preceding wave is, on average, related to the frequency bandwidth of the water surface elevation spectrum. Tromans et al. (1991) showed that a scaled sea state autocorrelation function (inverse Fourier transform of the water surface elevation spectrum) is an approximate model of the most probable shape of waves around an extreme event. This implies that the broader the bandwidth of the water surface elevation spectrum, the smaller, on average, will be the preceding wave. A Pierson Moscovitz spectrum (JONSWAP with peak enhancement factor, $\gamma=1$) representing a fully developed sea has a larger bandwidth than a JONSWAP spectrum ($\gamma>1$) for a developing storm. So, on average, the fully developed conditions make it easier for the highest wave in a wave group to impact on the cliff.

Fracturing of the cliff-top rock face occurs as a result of maximum impact pressure exceeding the tensile strength of the ignimbrite but the subsequent mode of detachment of the loosened block depends on the height and shape of the incident breaking wave. Three cases are now discussed in detail.

3.3.1. Incident breaking wave crests lower than cliff edge

The waves that cause damage to the cliff in this situation are relatively steep and this also affects the nature of the waves in front of the cliff. Using video footage (shown diagrammatically in Fig. 7),

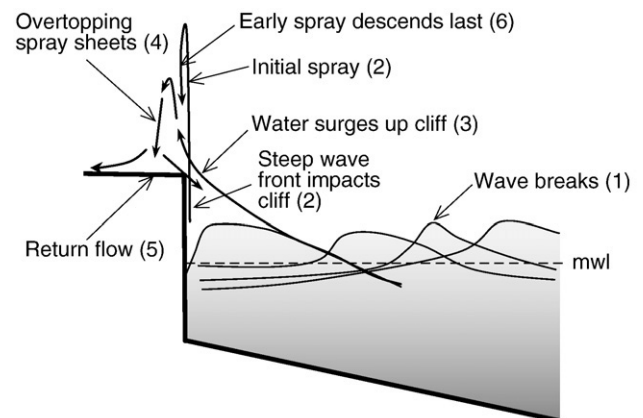


Fig. 7. Impact on cliff of a breaking wave of height lower than cliff edge height, $H = 12$ m, $T = 10$ s, ($1/13$ significant steepness).

typical steep wave impacts ($H=12$ m, $T=10$ s) on the cliff behave as follows:

1. Wave breaks over the top of the previous reflected wave and loses height before impacting the cliff;
2. On first impact, possibly lower down the cliff, a fast but thin vertical spray forms;
3. As the main body of the wave reflects from the cliff, the water surges up the cliff-face and may overtop it (linear theory predicts a doubling of wave height but non-linear effects may considerably increase the maximum elevation);
4. Overtopping results in a more substantial but slower moving sheet of spray inclined from the vertical towards the land (roughly bisecting the angle between cliff-face and the instantaneous water surface at the cliff-top). This corresponds with measured pressures on the cliff-top corner of, for example, 40 kPa (approximately 4 m head), directed approximately in the flow direction. The pressure within the spray sheet can lift and transport blocks;
5. Return flow from the overtopping descends onto the cliff-top some 5–10 m (full scale) landward of the cliff edge and flows back over the edge; and
6. Some of the early vertical spray sheet descends back onto the cliff edge producing large vertical impact forces where it lands.

The forces in the model tests were measured using a pressure-transducer panel located at the cliff-top corner. The natural period of the panel is about 0.04 s (model scale) or 0.3 s (full scale) and so does not measure very short duration pressure spikes. However, since the aim here was to assess whether a block will move or not, longer duration pressure loads are of more interest.

A typical vertical and horizontal pressure time history for a 14.4 m, 15 s wave impacting on a 15 m cliff is shown in Fig. 8 and can be cross-referenced with the incident wave behaviour shown in Fig. 9a,b,c. Fig. 9a shows the wave approaching the cliff with Fig. 9b showing an early stage of the impact as the crest surges up to the cliff-top, producing 4.3 m head of pressure. The vertical (upward) force occurs before the horizontal force starts to increase, a result of the initial flow being essentially vertical. However as the flow angle starts to rotate so the force rotates to have a landward component and the force on the corner becomes orientated at about 45° to the vertical (Fig. 9c). As the water falls back landward of the cliff edge the main force on the corner is from the substantial seaward-flow and it is orientated seaward at approximately 45° below the horizontal. Some of the fast-moving early spray sheet returns to the cliff edge quite late in this process and lands on the force transducer producing a 7 m head (Fig. 9d). Similar large vertical impacts have recently been noted during full-scale experiments on sea walls (Bullock et al., 2000; Wolters et al., 2005).

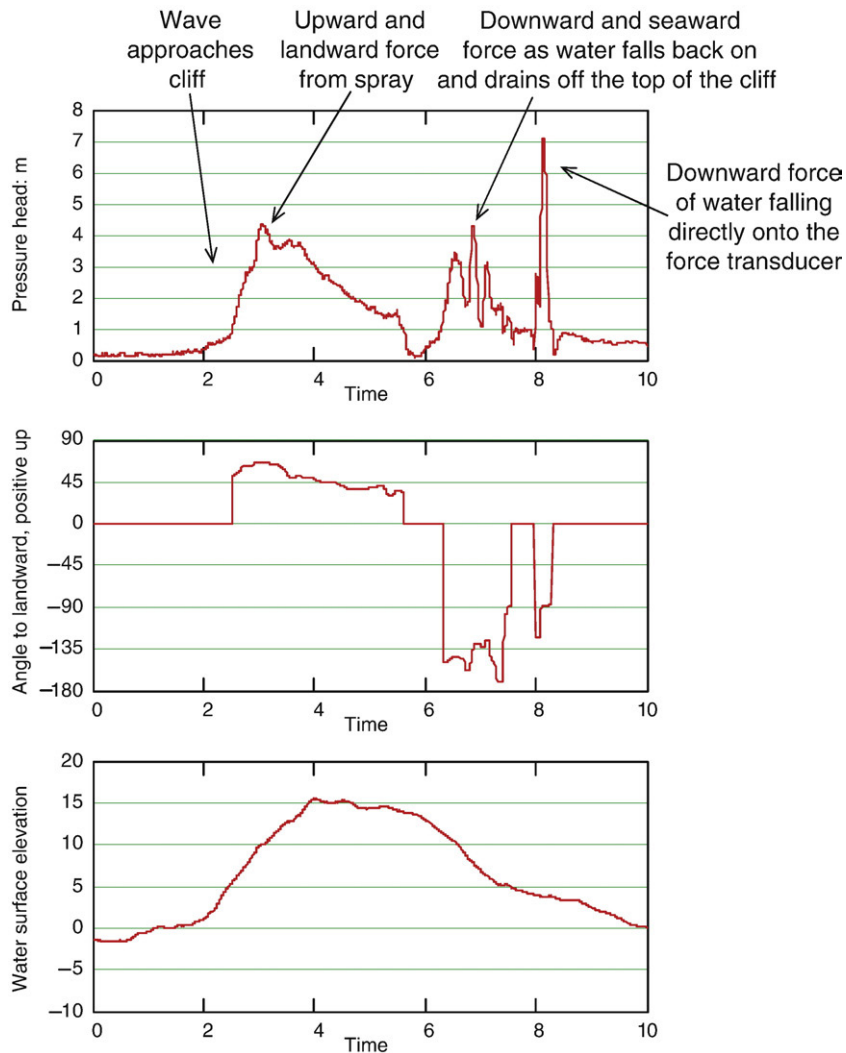


Fig. 8. Typical example of incident breaking wave crests lower than cliff edge: pressure, force direction and water surface elevation time histories ($H=14.4$ m, $T=15$ s, 1/24 significant steepness).

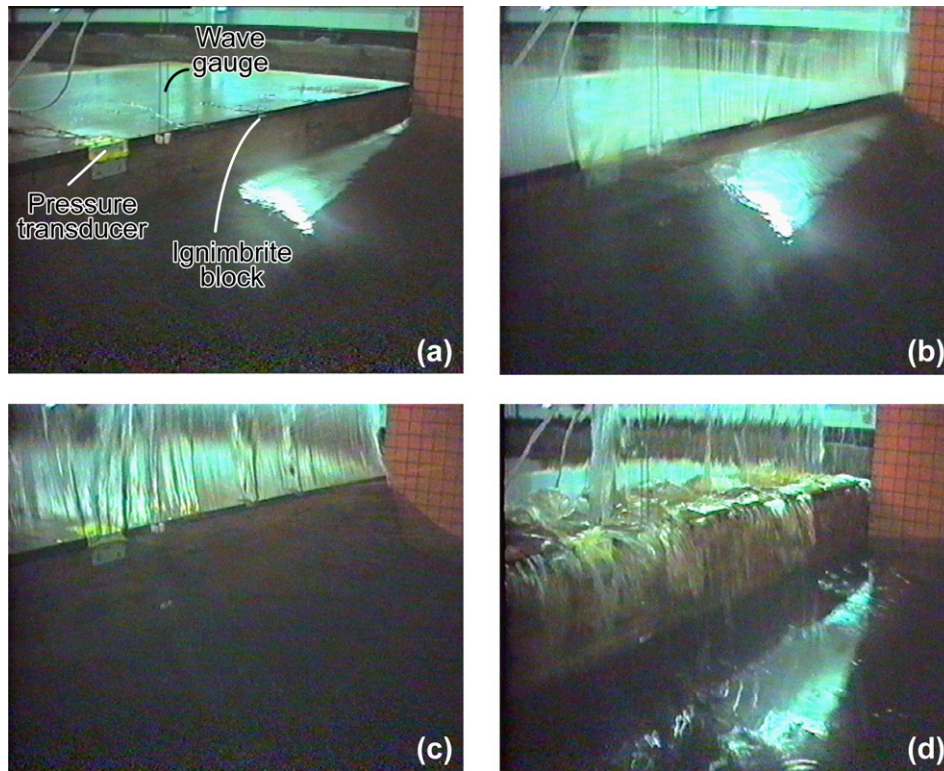


Fig. 9. Incident breaking wave height lower than the cliff edge. a: Video-still of steep wave crest approaching the model cliff showing pressure transducer, wire resistance gauge and ignimbrite block. b: Early wave impact and vertical spray sheet. c: Spray sheet angle at cliff edge rotates to 45°. d: Spray sheet descends, water drains from cliff. 1:60 scale tests.

In these tests the maximum impact pressures will have occurred well below the top of the cliff, yet the wave is still capable of lifting the block out of its cliff-top socket. The measured vertical suction pressures are about 4 m head. The block size that this will lift depends on whether the bottom of the block is also subject to hydrostatic/hydrodynamic forces. Assuming the block is not fully immersed, so that buoyancy forces do not affect the bottom face, this force is capable of lifting a 2 m × 1 m × 0.3 m block.

Pressure will not be uniformly distributed but is likely to be highest on the front edge and tend to lever the block out of its socket rather than lifting it directly. Larger forces would be expected if the block were subject to direct wave impact. The Grind ignimbrite blocks used in the model were carried by the flow landwards from the cliff edge by about 15 m (full scale) however, in some cases the block was then transported seaward over the cliff edge (Fig. 9d). Any protrusion of the block from the face of the cliff has an important effect on its movement. If it is slightly protruding from the face, it is subject to suction loading from the spray sheets and positive pressure in the void under the rock,

making the block more susceptible to movement by the incoming wave, greater landward movement occurs and there is much less likelihood of the block being subsequently transported seaward in the return flow. If the block is slightly recessed it may be protected from the highest velocities in the upward spray sheets but is more likely to be entrained by the outgoing flow over the cliff edge. In reality the cliff edge is irregular and the behaviour will depend on the shape of the cliff-face and whether the lower face of the block is shielded from the impacting wave.

3.3.2. Incident breaking wave crests level with cliff edge

Several factors make blocks more likely to be transported inland, and less likely to be washed back into the sea, when the incident waves are of approximately the same height as the cliff edge:

1. A higher incident wave crest relative to the cliff-top results in greater impact pressures and landward components;
2. A non-square cliff-top;

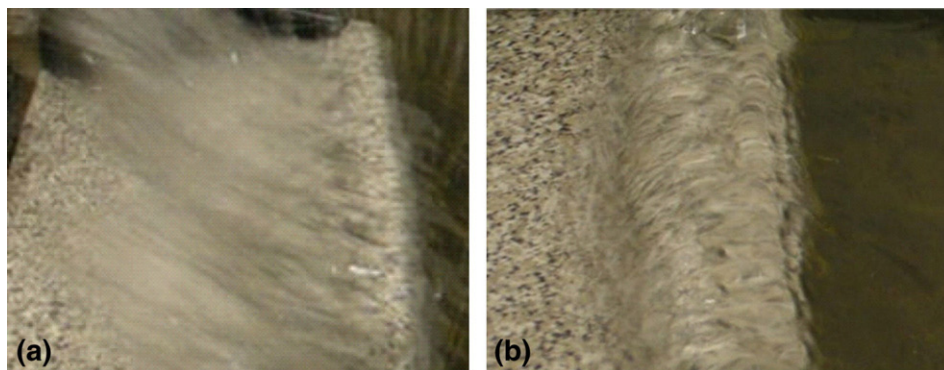


Fig. 10. a: Incident breaking wave height at same height as cliff edge with onshore deflected spray sheet. b: Incident wave higher than the cliff edge, overtopping has occurred and bore is about to form. 1:60 scale tests.

3. Inclination of the upper cliff-face landward; and
4. Interaction between the 3 dimensional nature of the real sea and the cliff-top may result in weaker return flow to the sea.

Small-scale tests were performed to investigate conditions 1 and 2. These demonstrated that for breaking waves with a crest elevation approximately equal to the cliff elevation, a major jet forms at approximately 45° to the horizontal and travels with a horizontal velocity approximately equal to the celerity of the incoming wave, transporting large volumes of water inland. Fig. 10a shows the inclined spray sheet from the case of a breaking wave with crest elevation at the cliff edge.

Breaking incident waves can form a bore in front of the cliff that impacts the cliff before any increase in height occurs. The impact pressures were not directly measured but spray heights of 120 m were observed. From ship bow impact tests (Xu and Barltrop, 2005) peak local pressures may be an order of magnitude greater than the spray heights and those higher local pressures would be capable of fracturing the rock and separating blocks from the cliff-face.

Numerical simulation of blocks entrained in flows demonstrates rapid acceleration up to approximately the flow speed, whereupon the block is essentially carried with the flow: a substantial jet of water accelerates the block and a substantial bore carries it landward. Entrained blocks are rarely carried as far as the water flow itself, because of the initial time taken to achieve entrainment and because flow velocity and depth will become insufficient in the later stages. Nevertheless, blocks can be carried large distances. The Grind ignimbrite blocks used in this test of the model were carried by the flow along a path landwards from the cliff edge by about 30 m (full scale). If there is no strong return flow, as a result of the 3-D shape of the cliff-top, the block would remain at the furthest point. However, if an intense return flow develops, as it did in the tests, then this can return the blocks seaward. Again any protrusion of the block from the face of the cliff affects its movement and slight protrusions from the face results in higher pressures, greater susceptibility to earlier movement, enhanced landward movement and a smaller likelihood of the block being washed back into the sea.

3.3.3. Incident non-breaking wave crests overtopping cliff edge

If the waves are less steep and higher than the cliff-top height, they do not break at the cliff and the resulting flow is different from the above situations. The principal differences in this set of tests were the non-breaking of the incident wave and the development of a substantial high velocity bore that transits across the cliff edge and top in a landward direction (see Figs. 10b and 11). The model tests show that:

1. The wave approaches the cliff and reflection and upward surge develops but no breaking occurs;
2. The surge overtops the cliff to form a fast bore flow and a slower moving wave crest that moves across the cliff-top as a solitary wave. See Fig. 10b, which shows the overtopping at stage 2 in Fig. 11;

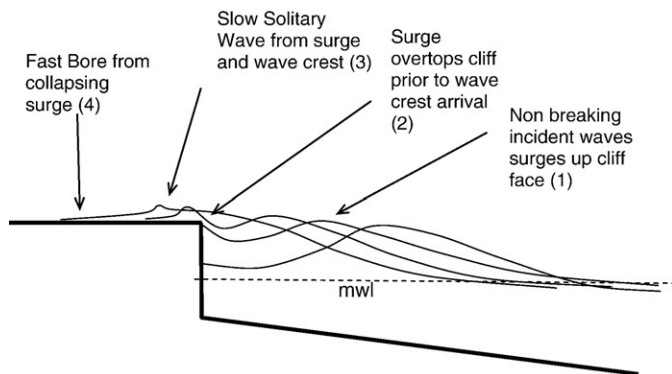


Fig. 11. High, non-breaking wave impacting on and over cliff (H=15 m, T=18 s, significant steepness=1/34).

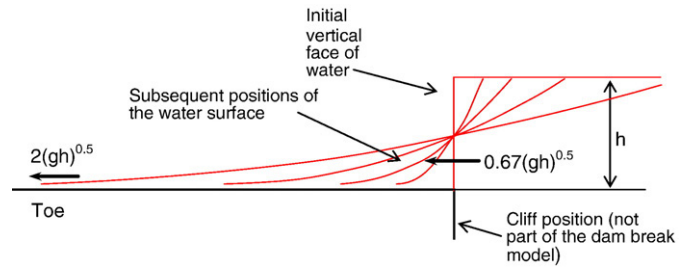


Fig. 12. Dam-break bore analogy to cliff overtopping by a wave.

3. The incident wave crest reaches the cliff-top, and if sufficiently high, coalesces with the cliff-top solitary wave; and
4. The bore continues across the cliff-top: if the cliff-top platform is upwards inclined the progress of the bore is limited by the flow energy; if the platform is flat viscous effects limit landward progress and the flow thickness declines.

3.4. Bore flow

The bore flow produced over the cliff-top by non-breaking overtopping waves is similar to the flow of green water on the deck of a ship, (investigated in the Safe-flow project (Buchner and Voogt, 2004; Safe-Flow, 2004)). The Safe-flow findings showed that a dam-break bore (flow commencing from a stationary vertical water wall) with velocity about \sqrt{gh} (where h is the depth of water overtopping the cliff edge) represented the hydrodynamics reasonably well. However, green water flow is closer to a dam break than the cliff-top flow because during a green water incident the ship is usually pitching and heaving downwards as the water surface moves upwards so that the bow cuts a wall in the water. In our tests, for the early part of the cliff flow the water tends to surge upwards and landwards onto the top of the cliff and then as the wave crest follows the surge there is an additional landward velocity.

We have used a theoretical solution (Henderson, 1966) for a dam-break bore on a smooth friction free level surface. This produces a rate of progress of the toe of water of $2\sqrt{gh}$, where h is the initial height of the water. However the average speed in the flow is lower and, averaged over a vertical section, increases linearly to this value from $\frac{2}{3}\sqrt{gh}$ at the cliff edge (position of original vertical face) as shown in Fig. 12. However, the appropriate velocity to use for calculation depends on the depth of the flow relative to the size of the block since a deep flow will completely surround the block and transport it closer to the bore toe and therefore within a faster flow.

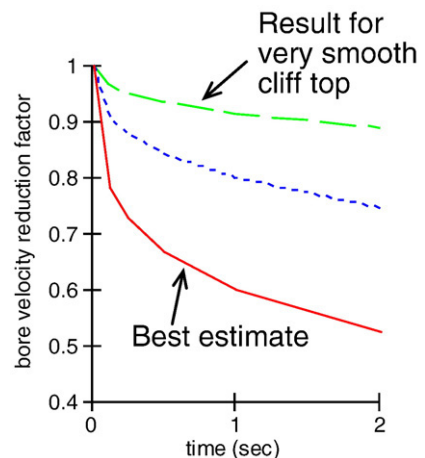


Fig. 13. Reduction in bore speed from $2\sqrt{gh}$, as a result of surface roughness.

Table 3
Speeds for different bore heights based on dam-break theory

Bore height (h)	Bore toe velocity $2\sqrt{gh}$	Average cliff edge velocity $\frac{2}{3}\sqrt{gh}$	Indicative velocity \sqrt{gh}
1 m	6.3 m s ⁻¹	2.1 m s ⁻¹	3.1 m s ⁻¹
5 m	14.0 m s ⁻¹	4.7 m s ⁻¹	7 m s ⁻¹
10 m	19.8 m s ⁻¹	6.6 m s ⁻¹	9.9 m s ⁻¹

The theoretical speed of a solitary wave (which the tests show to be similar to an initial dam-break flow) depends on the crest elevation η above the mean water level and is approximately $\sqrt{gd(1 + \frac{\eta}{2d})}$. If the crest elevation η = the water depth d and $h = d + \eta$, then the bore toe according to dam-break theory will travel at $2\sqrt{gh}$, whereas the solitary wave will travel at approximately $1.1\sqrt{gh}$. Both this fast bore and the slower cliff-top wave were observed in the wave-tank tests.

The surface over which the bore flows is rarely smooth and this reduces the bore speed (Witham, 1955). For a 5 m initial bore depth with different surface roughnesses the reduction in speed is shown by the lower curve in Fig. 13. However in the small, 1:375, Froude scaled lab tests with a smooth cliff-top the bore was not subject to the same frictional effects and travelled at a speed closer to the no friction value. In the small scale tests a long period wave with a crest elevation (and wave height) about equal to the 15 m cliff elevation produced a 4.5 m high bore travelling at a maximum velocity of 13.2 m s⁻¹, followed by a solitary wave travelling at 7.3 m s⁻¹. It should be noted that 15 m is not exceptionally large for the deep water offshore of Shetland where seas containing individual waves of this height might be expected to occur for about 100 h every year.

Whilst there is clearly some difficulty in choosing the most appropriate flow velocity for block transport calculations, in this paper an 'indicative' value of \sqrt{gh} is used.

Although the nearshore bathymetry data for The Grind is not fully known, the relatively deep water within a wavelength of the cliff-face suggests that waves in excess of 20 m regularly reach the cliff. Since the cliff at The Grind is 15 m high at its lowest, a 20 m wave elevation above still water level results in a bore of approximately 5 m high, travelling at toe velocity of 14 m s⁻¹ over the cliff-top. Other velocities and results for different bore heights are shown in Table 3. Morphological data from The Grind supports the modelling results and points to bores of varying height affecting the cliff-top (Hall et al., 2008).

The nature of the cliff-top slope will also affect the bore speed – a landward slope will compensate for the frictional effect and a suf-

ficiently steep slope will result in an accelerating flow. In contrast an upward slope will result in a deceleration and reduce the landward extent of the bore. Theoretically the initial condition for both the bore and the solitary wave are important: if the flow onto the cliff has a landward velocity then this would add to the velocity of both the bore and the solitary wave. If the incident wave is close to breaking, then the crest particle velocities are large and could significantly increase the flow speeds on the cliff. However in this case there is a tendency for spray sheets to form and to considerably modify the flow as discussed above.

3.5. Extraction of blocks from the cliff edge

It was demonstrated above that the forces experienced as waves impact at the cliff-face greatly exceed the rock strength, especially where the rock is fractured by previous wave impact. Noormets et al. (2004) consider a situation where a block is removed from the edge of a cliff. For a horizontal incident flow this is a similar problem to that considered in Section 3.7 for a block rolling out of a step.

In practice the flow is inclined upwards and the forces acting may be in the flow direction and hence drag rather than lift forces. In some circumstances the flow may pass the front surface of the block and hardly affect it. The simple lift-drag rolling model is therefore likely to be a poor estimator of the wave velocities required to move the top corner block. However the experiments demonstrated that a steep 12 m wave was capable of lifting the cliff edge block.

3.6. Transport of blocks by cliff-top bores

We propose that the following equations are relevant to the bore transport of a block over an approximately horizontal cliff-top such as occurs at Grind of the Navir and modelled here (Hall et al., 2006). Although hydrodynamic Munk moments will tend to orientate the block with the a -axis normal to the direction of movement, surface irregularities may well rotate it to other orientations and so transport with the a -axis parallel to flow is also considered (Fig. 14). Cliff-top obstacles may often inhibit progress of the block and so we consider situations where a block may:

1. slide over an unobstructed surface;
2. roll over a low obstacle; and
3. roll over a high obstacle.

The hydrodynamic forces acting on a block in the real environment are difficult to estimate with any accuracy because of the uncertainties

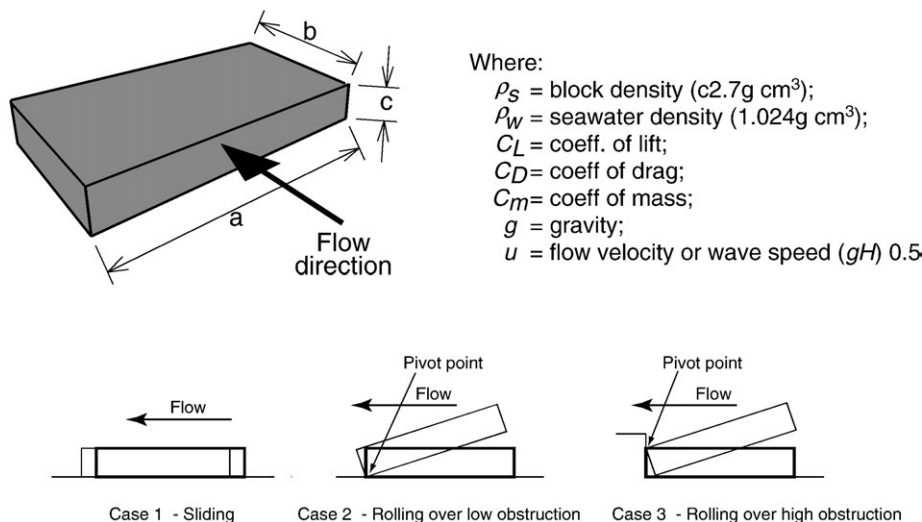


Fig. 14. Block dimensions and sliding and rolling modes.

in the flow, the orientation of the rock, whether there is a gap between the block and the cliff-top and the topography of the cliff-top over which the flow occurs before reaching the block. However the following analysis is attempted. Like Nott (2003), we consider lift and drag forces and moments but we use different estimates of the lift and drag coefficients and specifically consider two orientations A (*a*-axis parallel to flow) and B (*a*-axis normal to flow) and three transport modes described above. The assumption is made that the local flow depth is large in comparison with the block depth (*c*).

The drag coefficient is determined here for a prism in an unbounded flow with dimensions $b \times 2c$. The use of $2c$ rather than c accounts approximately for the effect of the bottom surface using a symmetry argument shown in Fig. 15. This gives a drag coefficient, C_D , of about 1.8 for orientation A and C_D about 1.3 for orientation B (following Barltrop and Adams, 1991). Comparison with measurements on buildings (Baines, 1963), shows that the overall C_D corresponds to a positive pressure on the front face that contributes over half of the drag force, but that the distribution can be very dependent on the turbulence levels in the incident flow.

The lift pressures will be very sensitive to the incident flow. Over most of the top surface a relatively small lift coefficient: C_{L1} taken as 0.1 occurs. It is assumed that a recirculation will occur behind the leading edge and this will lead to large lift coefficients in that area. An additional force corresponding to an additional lift coefficient of $C_{L2}=0.8$ applied as a rectangular pressure distribution over a length $c/2$ is assumed. However the overall flow pattern and lift coefficients will be sensitive to both plan and elevation fluid incidence angles, turbulence and upstream terrain. For example, it is well-known that flat roofs are subject to large lift pressures by wind when conical vortices form from the corners, when the flow is not parallel to an edge. (Note overall lift force measurements on blocks in a symmetric unbounded flow are not useful in this case because the overall C_L is zero.)

An additional correction is made for the three dimensional flows that will occur over the blocks, as opposed to the two-dimensional flows over the prisms that were the basis for the C_D calculation. The correction uses an effective width of block, estimated from pressure contours on buildings of:

$$a_e \quad a-b/2 \text{ for orientation A; and}$$

$$b_e \quad 0.75b \text{ for orientation B.}$$

We do not attempt to justify these precise values but it would not be reasonable to use prismatic coefficients without some finite width correction.

These assumptions are based on measurements of wind flow over buildings (Baines, 1963).

The resulting equations for cases 1, 2, and 3 with orientation A are:

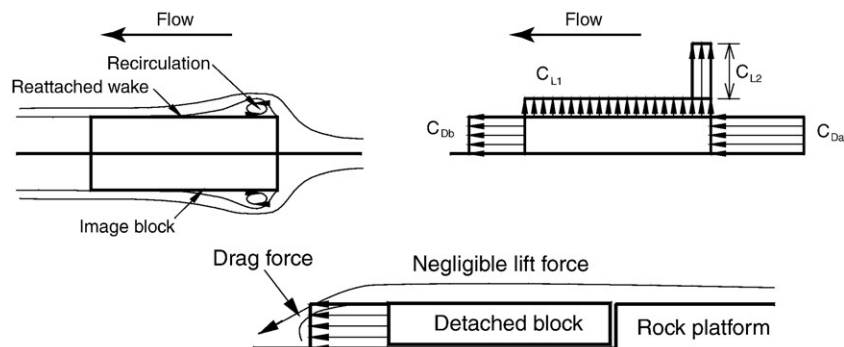


Fig. 15. Flow visualisation over block and pressure coefficients.

Table 4

Bore velocity (*v*) and bore height (*h*) required to transport a 2 m × 1 m × 0.3 m block

	Case 1: slide		Case 2: rotate low step		Case 3: rotate high step	
	(<i>v</i>)	(<i>h</i>)	(<i>v</i>)	(<i>h</i>)	(<i>v</i>)	(<i>h</i>)
Orientation A normal to flow	3.6 m s ⁻¹	1.3 m	5.1 m s ⁻¹	2.7 m	7.5 m s ⁻¹	5.8 m
Orientation B parallel to flow	5.4 m s ⁻¹	3.0 m	7.2 m s ⁻¹	5.3 m	8.0 m s ⁻¹	6.6 m

For sliding (case 1) the drag force must be greater or equal to the frictional force:

$$\frac{1}{2}\rho_w a_e c C_D v^2 \geq \mu \left[(\rho_r - \rho_w)(abc)g - \frac{1}{2}\rho_w a_e \left(b C_{L1} + \frac{c}{2} C_{L2} \right) v^2 \right]$$

or

$$v \geq \sqrt{\frac{[(\rho_r - \rho_w)(abc)g]}{\frac{1}{2}\rho_w a_e [c C_D + (b C_{L1} + \frac{c}{2} C_{L2})]}}$$

For overturning against a small obstacle (case 2) the drag overturning and lift overturning moments must exceed the weight restoring moment:

$$\frac{1}{2}\rho_w a_e \left[c C_D \left(\frac{c}{2} \right) + \left(b C_{L1} \frac{b}{2} + \frac{c}{2} C_{L2} \left(b - \frac{c}{4} \right) \right) \right] v^2 \geq [(\rho_r - \rho_w)(abc)g \frac{b}{2}]$$

or

$$v \geq \sqrt{\frac{[(\rho_r - \rho_w)(abc)g \frac{b}{2}]}{\frac{1}{2}\rho_w a_e \left[c C_D \left(\frac{c}{2} \right) + \left(b C_{L1} \frac{b}{2} + \frac{c}{2} C_{L2} \left(b - \frac{c}{4} \right) \right)]}}$$

Overturning against a large obstacle (case 3) is similar but the drag force now reduced to 60%, because it acts only on the upstream face and, because the block now has to pivot about its top, results in a restoring moment

$$\frac{1}{2}\rho_w a_e \left[-0.6c C_D \left(\frac{c}{2} \right) + \left(b C_{L1} \frac{b}{2} + \frac{c}{2} C_{L2} \left(b - \frac{c}{4} \right) \right) \right] v^2 \geq [(\rho_r - \rho_w)(abc)g \frac{b}{2}]$$

or

$$v \geq \sqrt{\frac{[(\rho_r - \rho_w)(abc)g \frac{b}{2}]}{\frac{1}{2}\rho_w a_e \left[-0.6c C_D \left(\frac{c}{2} \right) + \left(b C_{L1} \frac{b}{2} + \frac{c}{2} C_{L2} \left(b - \frac{c}{4} \right) \right)]}}$$

For orientation B the same equations can be used with b_e substituted for a_e , a substituted for b and with the appropriate value of C_D selected as discussed above.

The required bore height h at the cliff edge is estimated using the indicative velocity (see discussion above for likely range of velocities):

$$v = \sqrt{gh} \text{ or } h = \frac{v^2}{g}$$

Required velocities and bore heights to move a 2 m × 1 m × 0.3 m block are shown in Table 4.

An assumption was made that the flow depth was much larger than dimension c . Only for the minimum depth required for the 1A case (sliding with the long edge normal to the flow direction) is this assumption weak. On the basis of these calculations (which are sensitive to the input assumptions) flow depths at the cliff edge of about 7 m would comfortably transport the blocks via sliding and rotating over high obstacles. In the small scale tests a long period wave with a crest elevation about equal to the cliff elevation, of 15 m, produced a 4.5 m high bore. This is not a large wave for offshore Shetland (see above) and it follows that the 2.7 m high and 5.1 m s⁻¹ bore required to slide and where necessary rotate the blocks over low obstacles would be expected to occur often during severe storms and that 7 m bores are likely in the most severe storms. There will of course be some situations in which blocks cannot move with the flow: a step higher than about $b/2$ may allow a block to adopt a stable seaward-dipping position angled across the step.

3.7. Extraction of cliff-top blocks by the cliff-top bore

It has also been observed that blocks can be extracted from the cliff-top platform (Hall et al., 2006). The large vertical pressures sometimes associated with the falling spray sheets would certainly help to loosen these blocks although the susceptibility of the rock to jointing and fracturing is likely to contribute to block loosening and to then allow extraction by drag forces on the block.

Closed fractures in the rock face are widened by the removal of small rock chips, allowing the removal of small prismatic blocks from otherwise planar rock surfaces (Hall et al., 2008). This loss of small blocks is directly analogous to the loss of masonry blocks seaward from sea walls and breakwaters (Marth et al., 2005). New fracturing of *in situ* ignimbrite blocks forming the newly exposed faces of sockets at The Grind was observed in 2005 (Hall et al., 2008). Typically, curved fractures are developed across the bottom corners of blocks and fresh fractures in blocks above thin open horizontal joints indicates that hydraulic lift forces were sufficient to induce rock fracture or lift the block. Failed lifts are marked by chock stones holding open horizontal joints below blocks and by block edges displaced relative to bedrock joints.

Extraction of such blocks from the cliff-top platform is similar to the sliding case 1 above but the lift forces may be smaller (because the incident flow is parallel to the top surface) and the drag force significantly smaller (say 40%), (because the front face is below the incident flow).

The equations are

$$0.4\frac{1}{2}\rho_w a_e c C_D v^2 \geq \mu[(\rho_r - \rho_w)(abc)g]$$

or

$$v \geq \sqrt{\frac{[(\rho_r - \rho_w)(abc)g]}{0.4\frac{1}{2}\rho_w a_e c C_D}}$$

and results (for the 2 × 1 × 0.3 m block) in the velocities and required bore heights are shown in Table 5. The table suggests that under severe storms, most cliff-top platform sites will be susceptible to block extraction by moderate bore heights and velocities.

Table 5

Bore velocity (v) and height (h) required to extract a 2 m × 1 m × 0.3 m block from the landward side of a rock step on the cliff-top platform

	Bore velocity (v)	Bore height (h)
Orientation A, long axis normal to flow	6.5 m s ⁻¹	4.2 m
Orientation B, long axis parallel to flow	10.7 m s ⁻¹	11.7 m

3.8. Summary of experimental and numerical results

- Linear wave theory predicts that a wave incident normal to a cliff-face will reflect and double its height at the cliff-face. For the larger waves of interest, the non-linear behaviour is more complex and may involve:
 - large pressure loads on the cliff-face;
 - jet-formation at the cliff-face that may form a substantial spray sheet;
 - overtopping of the cliff to form a fast-moving bore over the cliff-top.
- Breaking waves can exert large pressures that are likely to extend pre-existing fractures in the cliff-face and promote the removal of blocks from the cliff-face and top.
- Blocks can be lifted and transported from the cliff-face and top by wave action.
- Steep, breaking waves with a crest elevation of about the cliff elevation can transport or throw blocks short distances inland.
- Where wave heights exceed cliff heights then cliff-top bores result in strong flows capable of removing blocks from the cliff-top and sliding and rolling them over substantial distances inland past obstacles.

4. Discussion

Assuming that unattenuated offshore extreme waves approach The Grind coast from the west-northwest and produce a spilling breaker of crest height about equal to the cliff elevation, our models indicate that the cliff-face can be subject to a steep wave front producing breaking wave impact forces on the cliff-face and quasi-steady flow forces on the cliff-top. Modelling the impact of large waves breaking against the cliffs has shown that as the lower part of the wave breaks on the structure, significant quantities of water contained in the upper part of the wave can surge upwards and landwards to form a spray sheet that lands to produce surface flow on the cliff-top that will move over the cliff in both landward and seaward directions. In situations where the incident wave crest elevation exceeds the cliff-top elevation, a high velocity bore of "green water" occurs, a process that we have confirmed in observation of the real cliff-top-flow behaviour in storm conditions. The latter phenomenon is also confirmed by observation as a process responsible for damage to the superstructures of offshore barge installations in both the North Sea and Western Atlantic (Safe-Flow, 2004). Our scale model tests demonstrate slightly different impact behaviour on cliffs because of the interaction with stronger wave reflections and because a downward moving bow is usually an important aspect of an offshore barge "green water" incident. However, in the absence of reflections which might break the waves earlier and reduce their intensity, steep fronted extreme waves remain highly damaging to the cliff-face because they result in the largest impact pressures.

High and breaking waves seem to explain the situation at The Grind where the orthogonal jointing of the local ignimbrites renders the cliff-face and top prone to fracture and easy detachment under storm conditions. Our modelling suggests that scaled breaking waves produce maximum local pressures of 7 MPa at the cliff-face (possibly reduced by surface effects to 3.5 MPa), but still well in excess of the 1.5 MPa tensile strength of the local rocks even when these are unfractured. Where pre-existing fractures exist from previous wave impact, the propagation of cracks enhances the potential for rock

failure (Noormets et al., 2004) and leads to greatly enhanced wave impact loads within the crack (Peregrine et al., 2004). However, we have not yet modelled these or performed wave-tank tests to relate the maximum socket size to the maximum size of block moveable under the modelled flow regime.

It appears increasingly clear from the field evidence in both Shetland and elsewhere (Hall et al., 2006, 2008) and the modelling results presented here of The Grind cliffs, that large waves and wave generated turbulent bores are capable of quarrying large boulders from the upper cliff-face, cliff-top edge and platform. Noormets et al. (2004) also showed this to be possible in Hawaii, where the bores from swell waves were capable of moving a 96 ton megaclast, albeit at the lower altitude of about 5 m a.s.l. However, they concluded that longer period waves, such as those produced by tsunami, were required to place and move the megaclasts on the platform in spite of also showing that the most recent 30 m movement of the megaclast to its present location did not coincide with the tsunami record. Nott (1997, 2004) has also drawn attention to the forms produced by some of the most powerful storms on earth on the western Australian coast, concluding in this location that none of these produced the enigmatic forms that are produced by tsunami. However, Nott (2004), acknowledges that waves from any source, including storms, are capable of producing the depositional and erosional forms that have been ascribed in the literature to tsunami (e.g. Bryant, 2001; Bryant and Haslett, 2007), particularly in locations where the nearshore water is of sufficient depth to allow the access of large storm waves.

This is the situation on many North Atlantic coasts where tsunami are rare (Dawson, 2000; Bondevik et al., 2005) yet extreme storm waves are common. Although incomplete, the sea level history of Shetland indicates a more or less continuous rise over the Holocene and recent times (Firth and Smith, 1993; Lambeck, 1993), suggesting that the CTSDs in Shetland are modern features increasingly accessed by large storm waves as water depths increase. CTSDs appear to be the product of extreme storm waves of dimensions and water levels not normally seen at the coast. That such waves are part of the deep water wave climate is now well-accepted (BPX, 1995; Lawton, 2001; Holliday et al., 2006) and it seems reasonable to assume that where nearshore water depths permit, these waves are largely unaffected by shoaling or refraction and may access the coast in a relatively unmodified form, remaining either unbroken or breaking very close to, or at, the cliff. If this is the case, then it also seems reasonable to assume that such waves will behave in ways that are relatively predictable. For example, if waves transport blocks over the top of the cliff, then these will be deposited at the limit of run-up to produce ridges composed of the population of boulder sizes in transport at the time. It might also be expected that the boulder ridges and imbricate clusters should broadly reflect the intricacies of the cliff-edge geometry as well as the wave approach directions. What appears to be most striking about the ridges and clusters of tabular imbricate boulders at The Grind is not only the altitude (15–20 m above sea level) and horizontal distance from the cliff edge (50–60 m inland), but also that the imbrication and organization into ridges approximates that seen in modern boulder beaches on cliff coasts where frequent rockfall results in weakly developed rounding (McKenna, 2005).

If these assumptions are accurate, and the cliff-top features of Shetland (and elsewhere) are indeed the product of modern extreme waves, then they are testimony to a major process affecting rock coasts that has had little systematic attention until recently (Hansom, 2001; Williams and Hall, 2004; Hall et al., 2006). Further, if the majority of erosional activity on storm-prone coasts fronted by deep water occurs in the upper parts of the cliff-face, cliff-top edge and cliff-top platform, with little evidence of comparable rates of erosion in the lower sections of the cliff-face, then the basal undercutting model of marine cliff evolution (e.g. Belov et al., 1999) does not apply here. Instead, the Shetland cliffs discussed above are essentially plunging forms (Trenhaile, 1987, 1997) that are low enough to allow extreme waves

of varying heights to overtop during major storms. As such the results here suggest that, where plunging cliffs are involved, models of cliff evolution need to accommodate erosion at the cliff-top edge and cliff-top platform and the transport of quarried debris inland.

5. Conclusions

This paper set out to clarify the morphogenetic and wave climate context of CTSDs, model wave conditions and forces encountered at the cliff-face and cliff-top platform and propose mechanisms to functionally link wave processes to the quarrying of blocks from the cliff-face and top, transport these blocks landwards over the cliff-top platform and deposit them at the rear of the cliff-top platform.

Our modelling has focussed on three situations where incident waves were lower than, at the same height as, and higher than the cliff edge height with results as follows:

1. Steep waves of 10 m and over on the 15 m high cliff result in considerable impact and lift forces on the upper cliff, with the resulting jets of water being capable of transporting large blocks. Laboratory scale experiments agree with full-scale experiments on seawalls elsewhere and demonstrate pressures sufficient to promote crack propagation, block detachment and lifting.
2. Large, but not necessarily steep, waves of the same height as the cliff produce sufficient impact pressures and water flow over the cliff edge and platform to entrain blocks and deposit them on the cliff-top, although return flows may return some blocks seawards.
3. Where cliff-top height is below wave crest elevation, “green water” flow occurs, similar to that experienced when waves exceed the bow freeboard of offshore vessels. On cliff-tops, loose blocks are subject to large lift and drag forces as the bore passes. Using pressure coefficients from steady flow past structures, lift forces well above the typical 0.5 ton block weight allow rotation or lifting of blocks out of cliff-top and cliff-top platform ‘sockets’. Drag forces from high flow velocities rapidly accelerate and transport blocks inland until the flow is attenuated by gradient and turbulent energy dissipation. Blocks are then deposited towards the limit of run-up as occurs in normal coarse clastic beach ridges.

The model results discussed above provides an explanatory framework to account for the fracturing of the upper part of the cliff-face and cliff-top platform under storm wave conditions and provide an insight into the exceptional velocities experienced over the cliff-top platform under bore flow conditions. Taken together, the modelling results point to an important geomorphological process that has previously been difficult to demonstrate or conceptualise in terms of nearshore wave behaviour. As a result erosion at the upper cliff, cliff-top edge and cliff-top platform and the transport of debris significant distances inland is absent from models of plunging cliff evolution. It is also clear from the above that the occurrence of substantial distributions of often imbricate quarried blocks, sited at altitudes not accessed by normal wave activity, are patently not exclusively tsunami-genic and so caution is required when using such evidence as diagnostic of palaeo-tsunami.

References

- Barltrop, N.D.P., Adams, A.J., 1991. The Dynamics of Fixed Marine Structures. Butterworth-Heinemann, Oxford.
- Baines, W.D., 1963. Effects of velocity distribution on buildings and structures. Proc Symposium on Wind Effects on Buildings and Structures, vol. 1. NPL, Teddington, UK.
- Barne, J.H., Robson, C.F., Kazanowska, S.S., Doody, J.P., Davidson, N.C., Buck, A.L. (Eds.), 1997. Coasts and Seas of the United Kingdom. Region 1 Shetland. Peterborough, Joint Nature Conservation Committee.
- Belov, A.P., Davies, P., Williams, A.T., 1999. Mathematical modelling of basal coastal cliff erosion in uniform strata: a theoretical approach. *J. Geol.* 107, 99–109.
- Bondevik, S., Mangerud, J., Dawson, S., Dawson, A., Lohne, O., 2005. Evidence for three North Sea tsunamis at the Shetland Islands between 8000 and 1500 years ago. *Quat. Sci. Rev.* 24, 1757–1775.

- BPX, 1995. BP Exploration. Report No: XFE/030/95 (Britannia Data Management, 628 Western Avenue, Park Royal, London).
- Bryant, E., 2001. Tsunami, the Underrated Hazard. Cambridge University Press, Cambridge. 320 pp.
- Bryant, E., Haslett, S., 2007. Catastrophic wave erosion, Bristol Channel, United Kingdom: impact of tsunami? *J. Geol.* 115, 253–269.
- Buchner, B.G., Voogt, A., 2004. Wave impacts due to steep fronted waves. Conference on Rogue Waves, Brest, Oct 2004.
- Bullock, G.N., Hewson, P.J., Crawford, A.R., Bird, P.A.D., 2000. Field and laboratory measurement of wave loads on vertical breakwaters. *Proceedings of Coastal Structures 99*, Balkema, Rotterdam, vol. 2, pp. 613–622.
- Burrige, D.M., 1973. London Weather Centre Memorandum No.22, London.
- Dawson, A.G., 2000. Tsunami risk in the northeast Atlantic region. Natural Environment Research Council, London. www.nerc-bas.ac.uk/tsunami-risks/html.
- Denny, D.F., 1951. Further experiments on wave pressures. *J. Inst. Civ. Eng.* 330–345 February.
- Gulev, S.K., Hasse, L., 1999. Changes of wind waves in the North Atlantic over the last 30 years. *Int. J. Climatol.* 19, 1091–1117.
- Gunther, H., Rosenthal, W., Stawartz, M., Carretero, J.C., Gomez, M., Lozano, I., Serrano, O., Reistad, M., 1988. The wave climate of the northeast Atlantic over the period 1955–1994: the WASA wave hindcast. *The Global Atmos. Ocean Syst.* 6, 121–163.
- Firth, C.R., Smith, D.E., 1993. Holocene sea level changes in Scotland. In: Birnie, J., Gordon, J., Bennett, K., Hall, A. (Eds.), *The Quaternary of Shetland*, Field Guide. Quaternary Research Association, Cambridge, p. 17.
- Hall, A.M., Hansom, J.D., Williams, D.M., Jarvis, J., 2006. Distribution, geomorphology and lithofacies of cliff-top storm deposits: examples from the high-energy coasts of Scotland and Ireland. *Mar. Geol.* 232, 131–155.
- Hall, A.M., Hansom, J.D., Jarvis, J., 2008. Patterns and rates of erosion produced by high energy wave processes on hard rock headlands: The Grind of the Navir, Shetland, Scotland. *Mar. Geol.* 248, 28–46.
- Hansom, J.D., 2001. Coastal sensitivity to environmental change: a view from the beach. *Catena* 42, 291–305.
- Hansom, J.D. and Hall, A.M., in press. Magnitude and frequency of extra-tropical North Atlantic cyclones: a chronology from cliff-top storm deposits. *Quaternary International*. doi:10.1016/j.quaint.2007.11.0.
- Hasselmann, K., Bamett, T.P., Bouws, E., Carlson, H., Cartwright, D.E., Enke, K., Ewing, J.A., Gienapp, H., Hassetmann, D.E., Kruseman, P., Meerburg, A., Mfiller, P., Olbers, K.J., Richter, K., Sell, W., Walden, W.H., 1973. Measurements of wind-wave growth and swell decay during the joint North Sea Wave Project (JONSWAP). *Dtsch. Hydrogr. Z., Erganz. A* 8 (12).
- Henderson, F.M., 1966. *Open Channel Flow*. Macmillan, New York.
- Holliday, N.P., Yelland, M.J., Pascal, R., Swail, V.R., Taylor, P.K., Griffiths, C.R., Kent, E., 2006. Were extreme waves in the Rockall Trough the largest ever recorded? *Geophys. Res. Lett.* 33, L05613.
- Homma, M., Horikawa, K., 1965a. Experimental study on total wave force against sea wall. *Coast. Eng. Jpn.* 8, 119–129.
- Homma, M., Horikawa, K., 1965b. Wave force against sea wall. *Proc 9th conf Coastal Engineering, ASCE*, pp. 490–503.
- Lambeck, K., 1993. Glacial rebound of the British Isles – II. A high-resolution, high precision model. *Geophys. J. Int.* 153, 960–990.
- Lawton, G., 2001. Monsters of the Deep. *New Sci.* 30, 28 June.
- Mactaggart, F., 1999. Villians of Hamnavoe and Esha Ness Coast SSSI's. Scottish Natural Heritage, Edinburgh.
- Marex, 1975. Report No. 172 (Marine Exploration Limited, Marex House, High St, Cowes, Isle of Wight.).
- Marth, R., Müller, G., Wolters, G., 2005. Damages of blockwork coastal structures due to internal wave impact induced pressures. *WIT Trans. Built Environ.* 79, 405–415.
- May, V., Hansom, J.D., 2003. Coastal geomorphology of Great Britain. *Geological Conservation Review Series*, No 28. Joint Nature Conservancy Council, Peterborough. 737 pp.
- McKenna, J., 2005. Boulder beaches. In: Schwartz, M.L. (Ed.), *Encyclopaedia of Coastal Science*. Springer, Dordrecht, pp. 206–208.
- Müller, G., Wolters, G., Cooker, M.J., 2003. Characteristics of pressure pulse propagation through water-filled cracks. *Coast. Eng.* 49 (1–2), 83–98.
- Noormets, R., Crook, K.A.W., Felton, E.A., 2004. Sedimentology of rocky shorelines: 3. Hydrodynamics of megaclast emplacement and transport on a shore platform, Oahu, Hawaii. *Sed. Geol.* 172, 41–65.
- Nott, J., 2003. Waves, coastal boulder deposits and the importance of the pre-transport setting. *Earth Planet. Sci. Lett.* 210, 269–276.
- Nott, J.F., 1997. Extremely high energy wave deposits inside the Great Barrier Reef Australia: determining the cause-tsunami or tropical cyclone. *Mar. Geol.* 14, 193–207.
- Nott, J.F., 2004. The tsunami hypothesis – comparisons of the field evidence against the effects, on the Western Australian coast, of some of the most powerful storms on Earth. *Mar. Geol.* 208, 1–12.
- Peregrine, D.H., Bredmose, H., McCabe, A., Bullock, G., Obhrai, C., Müller, Wolters, G., 2004. Violent water wave impact on walls and the role of air. In: Lisbon, McK., Smith, J. (Eds.), *Proc. 29th Internat. Conf. Coastal Engng.* World Science, vol. 4, pp. 4005–4017.
- Safe-Flow, 2004. Summary report on design guidance and assessment methodology for wave slam and green water impact loading. E.U. Project No. GRD1 2000-25656.
- Sunamura, T., 1992. *The Geomorphology of Rocky Coasts*. Wiley, Chichester, UK. 302 pp.
- Trenhaile, A.S., 1987. *The geomorphology of Clifed Coasts*. Clarendon Press, Oxford. 384 pp.
- Trenhaile, A.S., 1997. *Coastal Dynamics and Landforms*. Clarendon Press, Oxford. 366 pp.
- Trenhaile, A.S., Kanyaya, J., 2007. The role of wave erosion on sloping and horizontal shore platforms in macro-and mesotidal environments. *J. Coast. Res.* 23 (2), 298–309.
- Tromans, P.S., Anatürk, A.R., Hagameijer, P., 1991. A new model for kinematics of large ocean waves – application as a design wave. *Proc. First Int. Offshore and Polar Engineering, Conf. Edinburgh, UK*, pp. 64–71.
- Wang, D.W., Mitchell, D.A., Teague, W.J., Jarosz, E., Hulbert, M.S., 2005. Extreme waves under Hurricane Ivan. *Science* 309, 896.
- Williams, D.M., Hall, A.M., 2004. Cliff-top megaclast deposits of Ireland, a record of extreme waves in the North Atlantic – storms or tsunamis? *Mar. Geol.* 206, 101–117.
- Witham, G.B., 1955. The effects of hydraulic resistance in the dam-break problem. *Proceedings of the Royal Society of London. Series A. Mathematical and Physical Sciences (1934–1990)*, vol. 227. Number 1170. January.
- Wolters, G., Müller, G., Bruce, T., Obhrai, C., 2005. Large-scale experiments on wave downfall pressures. *Marit. Eng.* 158 (4), 137–145.
- Xu, L., Barltrop, N.D.P., 2005. *Wave Slap Loading on FPSO Bows*, HSE Books, HMSO. 0717629848.